

Infrared-Optical Double Resonance Spectroscopic Measurements and CCSD(T)/Complete Basis Set Limit Calculations on a Binary Complex between Phenylacetylene and Borane-trimethylamine. Understanding the Role of C–H···· π Interactions

Surajit Maity,^{†,#} Robert Sedlak,^{‡,#} Pavel Hobza,^{‡,¶,*} and G. Naresh Patwari^{†,*}

[†] Department of Chemistry, Indian Institute of Technology Bombay, Powai, Mumbai 400076 India.

[‡] Institute of Organic Chemistry and Biochemistry, Academy of Sciences of the Czech Republic and Center for Biomolecules and Complex Molecular Systems, Flemingovo nám. 2, 166 10 Prague 6, Czech Republic

[¶] Department of Physical Chemistry, Palacký University, 771 46 Olomouc, Czech Republic

[#] The contributions from Surajit Maity and Robert Sedlak are equal.

^{*} Authors to whom correspondence should be addressed. E-mail: hobza@uochb.cas.cz (P.H.); naresh@chem.iitb.ac.in (G.N.P.)

Abstract

The structure of the binary complex between phenylacetylene and borane-trimethylamine has been elucidated using IR-UV double resonance spectroscopy in combination with high-level ab initio calculations (CCSD(T) at complete basis set (CBS) limit). Borane-trimethylamine interacts primarily through multiple C–H $\cdots\pi$ interactions with the π electron density of the benzene ring in phenylacetylene. CCSD(T)/CBS level calculations provide reliable estimates for the interaction energy and free energy, which are in accord with the experimental observations. The DFT-SAPT calculations point out the dispersion along with electrostatics favor the formation of the experimentally observed complex.

Introduction

The nature of C–H $\cdots\pi$ interaction has been a subject of great interest due to its enormous implications in a variety of phenomena.¹ For instance, the gas phase structure of benzene dimer is a consequence of C–H $\cdots\pi$ hydrogen bonding.² However, the nature and orientation dependence of C–H $\cdots\pi$ interaction is not well understood in comparison with conventional hydrogen bonds. The monodentate structure of benzene methane cluster stabilizes via weak electrostatic interaction.³ On the other hand in the case of polycyclic aromatic ring the stability of the cluster and the orientation of the methane molecule is governed mainly by the dispersion forces.³ Nishio and co-workers have extensively investigated the role of C–H $\cdots\pi$ interactions in protein folding and its contribution to the stabilization of three dimensional structures of proteins and DNA.⁴ They have generalized that the C–H $\cdots\pi$ interaction originates primarily from the charge transfer process from

the π system to the anti-bonding orbital of the C–H bond with important contribution from the dispersion forces. The electrostatic contribution to the C–H $\cdots\pi$ interaction is usually unimportant except for species involving activated C–H groups, such as strong chloroform, acetylene.

In spite of their weakness, C–H $\cdots\pi$ interaction plays a crucial role in a variety of phenomena such as crystal packing, molecular recognition, protein folding, stereochemistry and others.¹ The specialty of C–H $\cdots\pi$ interaction is that it is primarily an interaction between a soft acid and a soft bases, wherein polarization and dispersion terms dominate.⁵ Vondrasek et al. have shown that stabilization energy inside hydrophobic core of a small protein has substantial contribution of C–H $\cdots\pi$ interactions involving side chains of aromatic residues.⁶ They have also shown that stabilization energy due to the dispersion interaction sometimes may have greater in energy compared to the conventional hydrogen bond. On the other hand, Harigai et al. have shown that loss of a single C–H $\cdots\pi$ interaction can cause substantial alteration of the stability and the photo-physical properties of photo-active yellow protein.⁷ In an interesting study Brandl et al. have shown that half of all aromatic rings in proteins act as hydrogen bond acceptors.⁸ Especially three quarters of all Trp rings and half of all Phe and Tyr rings and one quarter of all His rings are involved as hydrogen bond acceptors. Further, the interaction involving aliphatic C–H group with the π electron density of the aromatic ring are by far the largest set of C–H $\cdots\pi$ interactions (about 61.5%) observed in protein structures. In view of such observations a concerted experimental and theoretical effort to understand the C–H $\cdots\pi$ interactions are highly desirable. The motivation for this investigation is two-fold. First, the methyl groups on BTMA can mimic the interactions

of the aliphatic side chains with the aromatic rings, which in the present case is PHA. Secondly and more importantly, this investigation has added significance in view of the fact that PHA is a multifunctional molecule in the contest of hydrogen bonding, with the presence of two hydrogen bond acceptor groups in the form of π electron densities of the benzene ring and acetylenic $C\equiv C$ bond and the activated acetylenic $C-H$ group, which can act as hydrogen bond donor.

For the complete description of the complex between phenylacetylene (PHA) with borane-trimethylamine (BTMA) spectroscopic investigation in combination with high-level quantum mechanical ab initio calculations were carried out. These calculations can be used to determine the structures and estimate the stabilization energies. Since the differences in the interaction energies of various isomeric structures are expected to be rather small, therefore calculations were also carried out at very high theoretical level, where the uncertainty is small. Calculations using coupled-cluster CCSD(T) method combined with extended basis sets carried out and were extended to complete basis set (CBS) limit. These calculations though yield highly accurate total interaction energies, they however do not provide any information about the nature of stabilization. Hence, perturbation theory based energy decomposition analysis was also carried out.

Experimental and Computational Methods

The details of the experimental setup can be found elsewhere.⁹ Briefly, helium buffer gas was passed over PHA (Aldrich) kept in a solvent holder at room temperature and BTMA (Aldrich) sample chamber kept at 325K. The mixture was expanded through a 0.5 mm diameter pulsed nozzle (Series 9, Iota One; General Valve Corporation). PHA

and its complex with BTMA were excited using the frequency doubled output of a tunable dye laser (Narrow Scan GR; Radiant Dyes) pumped with second harmonic of a Nd:YAG laser (Surelite I-10; Continuum) and the ensuing total fluorescence was collected at right angles using a photo-multiplier tube (9780SB+1252-5F; Electron Tubes Limited) and a filter (WG-320) combination. The IR spectra of PHA and its BTMA complex were recorded using fluorescence dip infrared (FDIR) spectroscopic method.¹⁰ The source of tunable IR is an idler component of a LiNbO₃ OPO (Custom IR OPO; Euroscan Instruments) pumped with an injection-seeded Nd:YAG laser (Brilliant-B; Quatel). The typical energies used were about 100 μ J/pulse for the UV laser and about 2 mJ/pulse for the IR laser. The typical bandwidth of both UV and IR lasers is about 1 cm^{-1} and the absolute frequency calibration is within $\pm 2 \text{ cm}^{-1}$.

The structures of the monomers (PHA and BTMA) as well as the binary complexes were optimized without any constraints at the MP2 level using the aug-cc-pVDZ basis set. This level is known to provide accurate geometries of isolated systems as well as molecular complexes.¹¹ For faster convergence preliminary optimizations were carried out at MP2/6-31+G(d) level. The CCSD(T)/CBS binding energies were determined as a sum of MP2/CBS energies and CCSD(T) correction term.

$$\Delta E^{\text{CCSD(T)}}_{\text{CBS}} = \Delta E^{\text{MP2}}_{\text{CBS}} + (\Delta E^{\text{CCSD(T)}} - \Delta E^{\text{MP2}})|_{\text{medium basis set}}. \quad (1)$$

The method takes advantage of the fact that both the CCSD(T) and MP2 methods exhibit approximately the same basis set dependence.¹² Because of different dependence on the basis set the Hartree-Fock energies and MP2 correlation energies were extrapolated separately and using aug-cc-pVDZ and aug-cc-pVTZ basis sets. The extrapolations were

performed using the method proposed by Kim and coworkers,¹³ due to that fact that this extrapolation does not require a knowledge of any parameters unlike the like for Helgaker extrapolation.¹⁴ The present extrapolation is based on interaction energies corrected as well as uncorrected for the basis set superposition error and the assumption that both curves met in the CBS limit. The CCSD(T) correction term was determined with the aug-cc-pVDZ basis set. All interaction energies except those at CCSD(T)/CBS level were corrected for the basis set superposition error and the frozen core approximation was systematically used throughout the paper. The vibration frequency calculations were carried using MP2/aug-cc-pVDZ level and the resulting harmonic vibration frequencies was utilized without any scaling factors. Thermochemical analysis, based on rigid rotor – harmonic oscillator – ideal gas approximations, was carried out at the same level of theory.

Further, the DFT-SAPT (Symmetry Adapted Perturbation Theory) calculations were performed with the aug-cc-pVDZ basis set.¹⁵ This method allows for the separation of interaction energies into physically well defined components, such as those arising from electrostatic, induction, dispersion and exchange. The DFT-SAPT interaction energy (E^{int}) is given below.

$$E^{\text{int}} = E_1^{\text{Pol}} + E_1^{\text{Ex}} + E_2^{\text{Ind}} + E_2^{\text{Ex-Ind}} + E_2^{\text{D}} + E_2^{\text{Ex-D}} + \sigma\text{HF} \quad (2)$$

Equation 2 describes the electrostatic, exchange-repulsion, induction, exchange-induction, dispersion and exchange-dispersion terms, while the last term is a Hartree-Fock correction for higher-order contributions to the interaction energy. In the present

analysis the exchange-induction and exchange-dispersion terms will be included to the parent induction and dispersion terms. All calculations mentioned above were performed with the Gaussian-03 and Molpro suit of programs.^{16,17}

Results and Discussion

The fluorescence excitation spectra of PHA in the absence and in the presence of BTMA are shown in Figure 1. In both the spectra the intense peak at 35876 cm^{-1} is the band-origin transition of bare PHA.⁹ The addition of BTMA gives rise to appearance of new band at 35865 cm^{-1} , which can be assigned to the PHA-BTMA binary complex. This transition is shifted to the red by 11 cm^{-1} , relative to band-origin transition of bare PHA. In the case of complexes of PHA, it has been shown that it is difficult to correlate the intermolecular structures with the shifts in the electronic transitions.¹⁸ The observation of a new transition in the presence of BTMA provides the evidence of the formation of binary complex. In order to arrive at the intermolecular structure it is imperative to carry out the vibrational spectroscopic investigation in the acetylenic C–H stretching region. The FDIR spectra of PHA and PHA-BTMA complex were recorded by monitoring the fluorescence following excitation to the respective band-origin transitions at 35876 and 35865 cm^{-1} , respectively and the results are presented in Figure 2. The FDIR spectrum of PHA (Figure 2A) shows two strong transitions at 3325 and 3343 cm^{-1} which has been assigned as the Fermi resonance bands between the C–H stretching vibration and a combination of one quantum of $\text{C}\equiv\text{C}$ stretch and two quanta of C–H out-of-plane bending mode and other weak features to the transitions arising out of higher order coupling terms.¹⁹ Surprisingly, the FDIR spectrum of PHA-BTMA (Figure 2B) also shows two

intense transitions at 3327 and 3339 cm^{-1} . This spectrum clearly shows the presence of Fermi resonance bands, albeit with some minor changes in the position and relative intensities of the two bands. Further the weaker band observed at 3313 cm^{-1} can be assigned to transitions arising out of higher order coupling terms, similar to bare PHA.¹⁹ The FDIR spectrum of PHA-BTMA complex clearly indicates that the acetylenic C–H group of PHA remains unperturbed in spite of its interaction with BTMA. This implies that the formation of a C–H \cdots H–B dihydrogen-bonded complex, wherein the acetylenic C–H group of PHA moiety interacts with the BH_3 group of BTMA, similar to acetylene-BTMA complex,²⁰ can be ruled out. Comparison with the other hydrogen-bonded complexes of PHA indicates that BTMA primarily interacts with the π electron density of the benzene ring in PHA.^{18,21,22}

Ab initio calculations were carried out to supplement the experimental observations. Several initial structures were randomly generated, which contained both hydrogen-bonded as well as stacked motifs and these structures were pre-optimized at MP2/6-31+G(d) level. The final optimizations followed by vibrational frequency calculations were performed at MP2/aug-cc-pVDZ level. These calculations resulted in two unique structures, which are depicted in Figure 3. The first complex (A) is characterized by the presence of C–H \cdots H–B dihydrogen bonding, stabilized by interaction between two oppositely charged hydrogen atoms on PHA and BTMA. The intermolecular structure of this complex is very similar to acetylene-BTMA complex,²⁰ with the presence of a pair of symmetrically bifurcated dihydrogen bonds with the H \cdots H contact distance of 2.32 Å. The C–H \cdots H–B distances are marginally longer in the PHA-BTMA in comparison with acetylene-BTMA complex (2.27 Å at MP2/aug-cc-pVDZ

level), which can be attributed to the lowering of the acidity of the C–H group due to the presence of phenyl group.

On the other hand the second complex (**B**) has multiple C–H $\cdots\pi$ interactions between the methyl C–H groups and the π electron density of the benzene ring in PHA. Interestingly one of the methyl C–H groups points to the center of the benzene ring. As mentioned earlier the Fermi resonance bands in PHA arise due to the coupling between one quantum of C \equiv C stretch and two quanta of C–H out-of-plane bending mode.¹⁹ Any perturbation to either the C \equiv C and/or C–H oscillator will result in loss of Fermi resonance. The FDIR spectrum of PHA-BTMA complex, depicted in Figure 2B, thus rules out the interaction of BTMA with both acetylenic C–H and C \equiv C oscillators. The interaction with C–H oscillator with the BH₃ group of BTMA results in formation of a C–H \cdots H–B dihydrogen-bonded complex, similar to the structure shown in Figure 3A. The formation of this complex can be completely ruled out, since this would have lead to substantial lowering of the acetylenic C–H stretching frequency, similar to PHA-ammonia complex.¹⁸ The frequency calculations at MP2/aug-cc-pVDZ level, listed in Table 1, indicate that formation of C–H \cdots H–B would have lowered the acetylenic C–H stretching frequency by about 50 cm^{–1}. Further, the interaction of BTMA with the acetylenic C \equiv C oscillator can also be ruled out as this would have lead to loss of Fermi resonance band, similar to PHA-water complex.²¹ Thus the FDIR spectrum of PHA-BTMA complex, depicted in Figure 2B, clearly indicates that BTMA interacts primarily with π electron density of the benzene ring in PHA leading to formation of a complex, similar to that shown in Figure 3B. Further, it can be seen from Table 1 that calculated (unscaled) C–H vibrational frequencies of the complex **B**, unlike complex **A**, change very

marginally with respect to bare PHA and hence would retain the Fermi resonance couplings.

The FDIR spectrum and the vibrational frequency calculations clearly and unambiguously assign the observed PHA-BTMA complex to the structure shown in Figure 3B, which is stabilized by multiple C–H $\cdots\pi$ interactions. The observation of this structure of surprising based on the fact that the proton affinities of BTMA (838.6 kJ mol⁻¹) and ammonia (853.6 kJ mol⁻¹) are very close and the fact that ammonia forms a C–H \cdots N hydrogen bonded complex with PHA.^{23,24} This implies that the multiple C–H $\cdots\pi$ interactions, which are characteristic for structure **B** should be energetically more favorable than C–H \cdots H–B interaction present in structure **A**. In order to understand the origin of this behavior, the stabilization energies at various levels of theory were calculated and the results are listed in Table 2. In all cases the stabilization energies were corrected for zero point energy (ZPE) and basis set superposition error (BSSE). At the MP2/aug-cc-pVDZ level the complex **B** is more stable by about 4 kJ mol⁻¹ relative to complex **A**. This is in good agreement with the present experimental finding. However, it is well known that MP2 level calculations overestimate the dispersion energies and single point calculations at CCSD(T) level would provide a more accurate description.²⁵ Single point calculations were also carried out using CCSD(T)/aug-cc-pVDZ level calculations for the MP2/aug-cc-pVDZ optimized structures. At the CCSD(T)/aug-cc-pVDZ level both the structure are almost isoenergetic, with complex **A** being very marginally (0.2 kJ mol⁻¹) more stable than complex **B**. Given that complex **B** is exclusively observed experimentally, the CCSD(T) level calculations are not in good agreement with the experimental results. Similar results were obtained for the DFT-SAPT calculations,

wherein the difference between the energies of complex **A** and complex **B** are very marginal. However at the highly accurate CCSD(T)/CBS theoretical level, the observed complex **B** is stable over the complex **A** by about 2 kJ mol⁻¹.

Since the temperature of the experiment is non-zero (see later) it is necessary to evaluate the free energy surface which includes the entropy contribution. The Gibbs free energy (ΔG) for the formation of the two complexes **A** and **B** as a function of temperature (T) are presented in Figure 4. The ΔG values were obtained by the thermochemical analysis following vibrational frequency calculations in Gaussian-03 at MP2/aug-cc-pVDZ level of theory, with the electronic energy obtained at CCSD(T)/CBS level. This plot reveals that the ΔG for the formation of both the complexes is positive for temperatures above ~110 K. Interestingly, the ΔG for the formation of complex **B** becomes more negative than for complex **A** below ~90 K. At 10 K, which is close to the final temperature for the present experiments,²⁶ the formation of complex **B** ($\Delta G = 15.7$ kJ mol⁻¹) is favored over the formation of complex **A** ($\Delta G = 12.8$ kJ mol⁻¹), which is in accord with the experimental observations.²⁷

The DFT-SAPT interaction energy decomposition was carried out for the two PHA-BTMA complexes using aug-cc-pVDZ basis set and the results are presented in Table 3. For the complex **A**, the electrostatic contribution (-20.8 kJ mol⁻¹) is slightly higher than the dispersion component (-16.4 kJ mol⁻¹), while the induction contribution is very minor (-2.6 kJ mol⁻¹). Surprisingly, the electrostatic contribution of -21.4 kJ mol⁻¹ in complex **B** is similar in magnitude to the electrostatic contribution in complex **A**. On the other hand the dispersion has much larger contribution of -34.3 kJ mol⁻¹, supported by much smaller contribution of -2.5 kJ mol⁻¹ from induction. However, the large positive

contribution from the exchange energy of 47.3 kJ mol^{-1} for the complex **B** compensates for the higher contributions due to dispersion and electrostatic forces. As a result the DFT-SAPT electronic interaction energies for both the complexes are nearly equal (see Table 3). The situation remains unchanged even after ZPE correction (see Table 2). Further, the DFT-SAPT stabilization energies are comparable to the ZPE and BSSE corrected CCSD(T) energies using the same basis set (see Table 2). However, in the present case both DFT-SAPT/aug-cc-pVDZ and CCSD(T)/aug-cc-pVDZ methods underestimate the binding energies when compared to the CCSD(T)/CBS results. This finding is in agreement with that reported by Hesselmann and Jansen.²⁸ The DFT-SAPT calculations clearly indicate that the multiple $\text{C-H}\cdots\pi$ hydrogen-bonded PHA-BTMA complex is stabilized primarily through dispersion interaction with significant contribution from electrostatic interaction and very small contribution due to induction.

Conclusions

The fluorescence excitation spectrum of PHA in the presence of BTMA reveals the formation of a binary complex, whose electronic transition is shifted to the red by 11 cm^{-1} , relative to bare PHA. The FDIR spectrum of PHA-BTMA complex in the acetylenic C-H stretching region is very similar to the corresponding spectrum of PHA, which clearly indicates that BTMA is not interacting with the acetylenic $\text{C}\equiv\text{C}$ and C-H groups. The inability of BTMA to form $\text{C-H}\cdots\text{H-B}$ dihydrogen-bonded complex was rather surprising, in view of the fact that the proton affinity of BTMA is very close to that of ammonia. Two unique PHA-BTMA complexes were optimized using MP2/aug-cc-pVDZ level of theory. The first one is characterized by the presence of symmetrically bifurcated

C–H \cdots H–B dihydrogen bonding, while the second complex shows multiple C–H $\cdots\pi$ contacts. Both the complexes were found to be almost isoenergetic using single point calculations at CCSD(T)/aug-cc-pVDZ level. However, at CCSD(T)/CBS level the C–H $\cdots\pi$ hydrogen-bonded complex is the most stable complex. The free energy calculations unambiguously favor the formation of C–H $\cdots\pi$ hydrogen-bonded at temperatures closer to the experimental conditions. The DFT-SAPT calculations reveal that dispersion along with electrostatics play vital role in stabilizing the experimentally observed complex. Finally, for systems wherein competitive interactions with large contribution for dispersion forces are involved, very high levels of theory are required to accurately describe the system.

Acknowledgements. Authors wish to thank Mr. Prashant Chandra Singh for his help rendered during the experiments and Mr. Atanu Bhattacharya for initial calculations. This material is based upon work supported by Department of Science and Technology (Grant No.SR/S1/PC/23/2008), Council of Scientific and Industrial Research (Grant No. 01(2268)/08/EMR-II) and Board of Research in Nuclear Sciences (Grant No. 2004/37/5/BRNS/398) to G.N.P. S.M. thanks UGC for the Junior Research Fellowship. This work is part of the research project Z4 055 905 and is supported by grants from Ministry of Education of the Czech Republic (Center for Biomolecules and Complex Molecular Systems, LC512 and MSM6198959216). The support from Praemium Academiae, Academy of Sciences of the Czech Republic dedicated to P.H. in 2007 is also acknowledged.

References and Notes

- (1) Nishio, M.; Hirota, M.; Umezawa, Y. *The CH/ π interaction*; Wiley-VCH: New York, 1998.
- (2) Arunan, E.; Gutowsky, H. S. *J. Chem. Phys.* **1993**, *98*, 4294.
- (3) Tsuzuki, S.; Fujii, A. *Phys. Chem. Chem. Phys.*, **2008**, *10*, 2584. (b) Tsuzuki, S.; Honda, K.; Fujii, A.; Uchimaru, T.; Mikami, M. *Phys. Chem. Chem. Phys.*, **2008**, *10*, 2860.
- (4) Nishio, M.; Umezawa, Y.; Hirota, M.; Takeuchi, Y. *Tetrahedron*, **1995**, *51*, 8665.
- (5) Gil, A.; Branchadell, J. B.; Bertran, J.; Oliva, A.; *J. Phys. Chem. B*, **2007**, *111*, 373.
- (6) Vondrasek, J.; Bendova, L.; Klusak,; Hobza, P. *J. Am. Chem. Soc.*, **2005**, *127*, 2615.
- (7) Harigai, M.; Kataoka, M.; Imamoto, Y. *J. Am. Chem. Soc.* **2006**, *128*, 10646.
- (8) Brandl, M.; Weiss, M. S.; Jabs, A.; Suhnel, J.; Hilgenfeld, R. *J. Mol. Biol.* **2001**, *307*, 357.
- (9) Singh, P. C.; Patwari, G. N. *Curr. Sci.* **2008**, *95*, 469.
- (10) Page, R. H.; Shen, Y. R.; Lee, Y. T. *J. Chem. Phys.* **1988**, *88*, 4621.
- (11) Dabkowska, I.; Jurecka, P.; Hobza, P. *J. Chem. Phys.* **2005**, *122*, 204322.
- (12) Jurecka, P.; Hobza, *Chem. Phys. Lett.* **2002**, *365*, 89.

- (13) Lee, E. C.; Kim, D.; Jurecka, P.; Tarakeshwar, P.; Hobza, P.; Kim, K. *S. J. Phys. Chem. A* **2007**, *111*, 3446.
- (14) Halkier, A.; Helgaker, T.; Jorgensen, P. Klopper, W. Koch, H. Olsen, J. Wilson, A. K. *Chem. Phys. Lett.* **1998**, *286*, 243.
- (15) (a) Jeziorski, B.; Moszynski, R.; Szalewicz, K. *Chem. Rev.* **1994**, *94*, 1887. (b) Hesselman, A.; Janssen, G.; Schutz, M. *J. Chem. Phys.* **2005**, *122*, 14103.
- (16) Frisch, M. J. Trucks, G. W.; Schlegel, H. B.; Scuseria, G. E.; Robb, M. A.; Cheeseman, J. R.; Montgomery, J. A., Jr.; Vreven, T.; Kudin, K. N.; Burant, J. C.; Millam, J. M.; Iyengar, S. S.; Tomasi, J.; Barone, V.; Mennucci, B.; Cossi, M.; Scalmani, G.; Rega, N.; Petersson, G. A.; Nakatsuji, H.; Hada, M.; Ehara, M.; Toyota, K.; Fukuda, R.; Hasegawa, J.; Ishida, M.; Nakajima, T.; Honda, Y.; Kitao, O.; Nakai, H.; Klene, M.; Li, X.; Knox, J. E.; Hratchian, H. P.; Cross, J. B.; Bakken, V.; Adamo, C.; Jaramillo, J.; Gomperts, R.; Stratmann, R. E.; Yazyev, O.; Austin, A. J.; Cammi, R.; Pomelli, C.; Ochterski, J. W.; Ayala, P. Y.; Morokuma, K.; Voth, G. A.; Salvador, P.; Dannenberg, J. J.; Zakrzewski, V. G.; Dapprich, S.; Daniels, A. D.; Strain, M. C.; Farkas, O.; Malick, D. K.; Rabuck, A. D.; Raghavachari, K.; Foresman, J. B.; Ortiz, J. V.; Cui, Q.; Baboul, A. G.; Clifford, S.; Cioslowski, J.; Stefanov, B. B.; Liu, G.; Liashenko, A.; Piskorz, P.; Komaromi, I.; Martin, R. L.; Fox, D. J.; Keith, T.; Al-Laham, M. A.; Peng, C. Y.; Nanayakkara, A.; Challacombe, M.; Gill, P. M. W.;

Johnson, B.; Chen, W.; Wong, M. W.; Gonzalez, C.; Pople, J. A.
Gaussian 03, Revision A.1; Gaussian, Inc.: Wallingford, CT, 2003.

- (17) (14) MOLPRO, a package of *ab initio* programs designed by Werner H. J. and Knowles, P. J. version 2006.1, Amos, R. D.; Bernhardsson, A.; Berning, A.; Celani, P.; Cooper, D. L.; Deegan, M. J. O.; Dobbyn, A. J.; Eckert, F.; Hampel, C.; Hetzer, G.; Knowles, P. J.; Korona, T.; Lindh, R.; Lloyd, A. W.; McNicholas, S. J.; Manby, F. R.; Meyer, W.; Mura, M. E.; Nicklass, A.; Palmieri, P.; Pitzer, R.; Rauhut, G.; Schuřtz, M.; Schumann, U.; Stoll, H.; Stone, A. J.; Tarroni, R.; Thorsteinsson, T. and Werner, H.-J.
- (18) Singh, P. C.; Patwari, G. N.; *J. Phys. Chem. A*, **2008**, *112*, 4426.
- (19) Stearns, J. A.; Zwier, T. S. *J. Phys. Chem. A*, **2003**, *107*, 10717.
- (20) Singh, P. C.; Patwari, G. N. *Chem. Phys. Lett.* **2006**, *419*, 5.
- (21) Singh, P. C.; Bandyopadhyay, B.; Patwari, G. N. *J. Phys. Chem. A* **2008**, *112*, 3360.
- (22) Singh, P. C.; Patwari, G. N.; *J. Phys. Chem. A*, **2008**, *112*, 5121.
- (23) Patwari, G. N. *J. Phys. Chem. A* **2005**, *109*, 3360.
- (24) Hunter, E. P. L.; Lias, S. G. *J. Phys. Chem. Ref. Data* **1998**, *27*, 413.
- (25) (a) Janowski, T.; Pulay, P. *Chem. Phys. Lett.* **2007**, *447*, 27. (b) Jureřka, P.; řponer, J.; řerný, J.; Hobza, P. *Phys. Chem. Chem. Phys.* **2006**, *8*, 1985.

- (26) The band-shape of the origin band of PHA-BTMA complex was analyzed and from the width the rotational temperature was estimated to be around 3.5K.
- (27) With the difference in ΔG of 2.9 kJ mol^{-1} between the two complexes, at 10 K the Boltzmann population distribution will exclusively favor formation of complex **B**.
- (28) (a) Jansen, G.; Hesselmann, A. *J. Phys. Chem. A* **2001**, *105*, 11156. (b) Hesselmann, A.; Jansen, G. *Phys. Chem. Chem. Phys.* **2003**, *5*, 5010.

1. **Figure 1.**

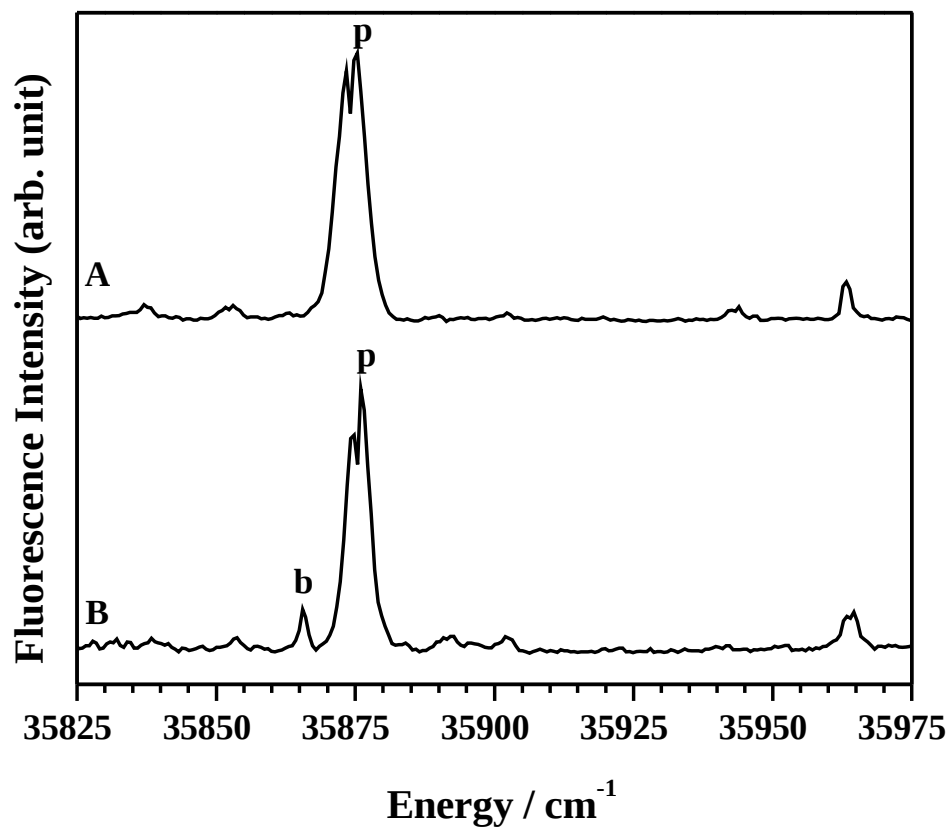


Figure 1. Fluorescence excitation spectra of (A) phenylacetylene and (B) phenylacetylene in the presence of BTMA. In both the traces the peaks marked with “p” and “b” are the band-origin transitions for phenylacetylene and phenylacetylene-BTMA, respectively.

Figure 2.

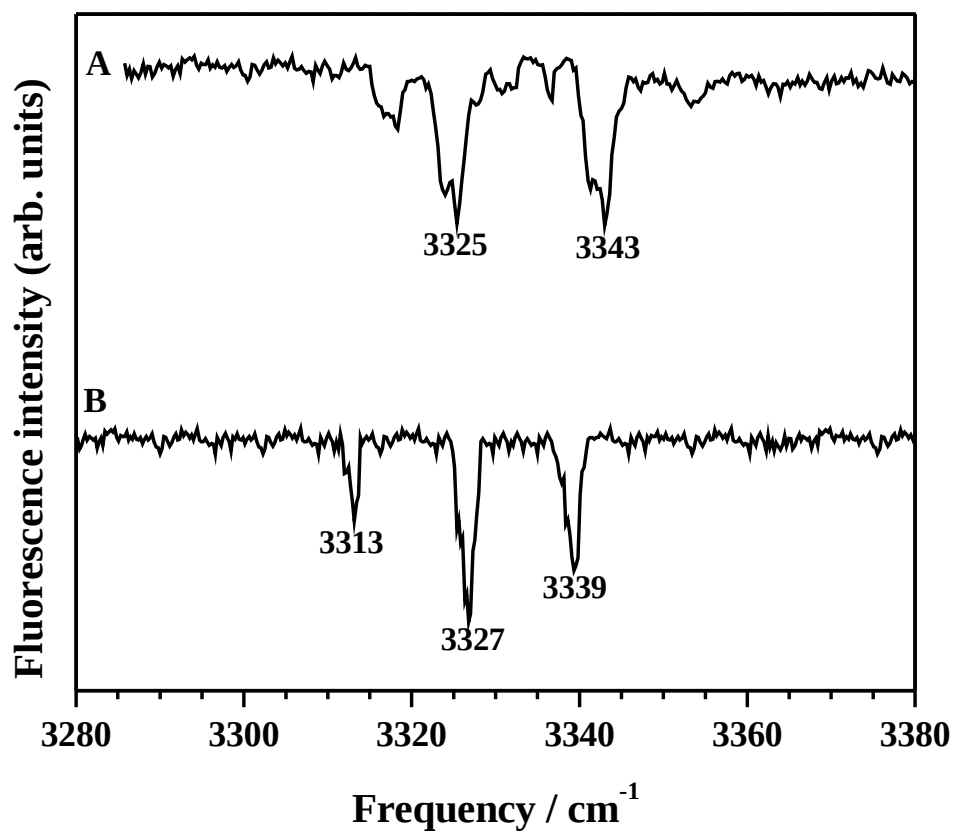


Figure 2. FDIR spectra of (A) phenylacetylene and (B) phenylacetylene-BTMA in the acetylenic C–H stretching region.

Figure 3.

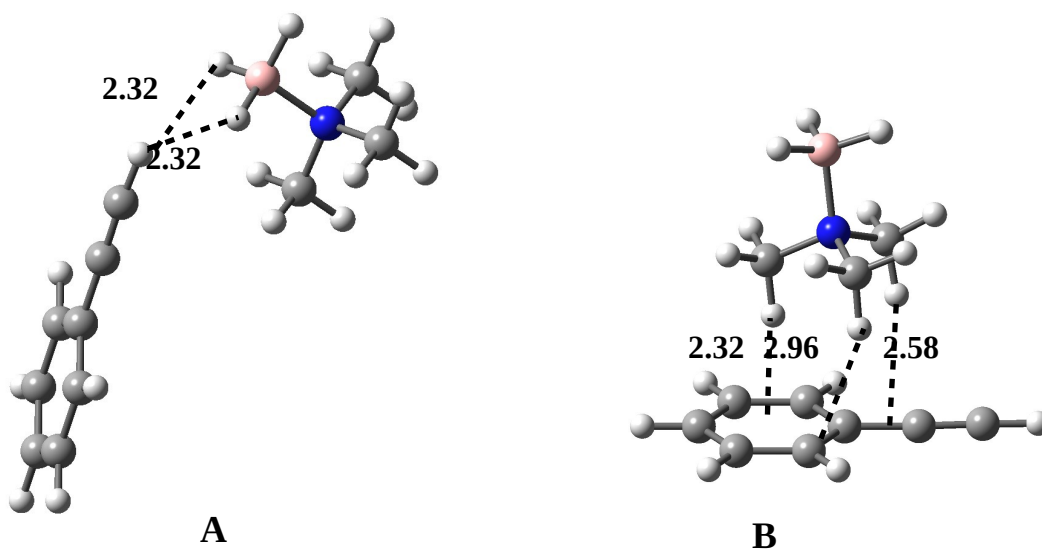


Figure 3. Structures of PHA-BTMA complexes calculated at MP2/aug-cc-pVDZ level.

Distances are given in angstroms.

Figure 4.

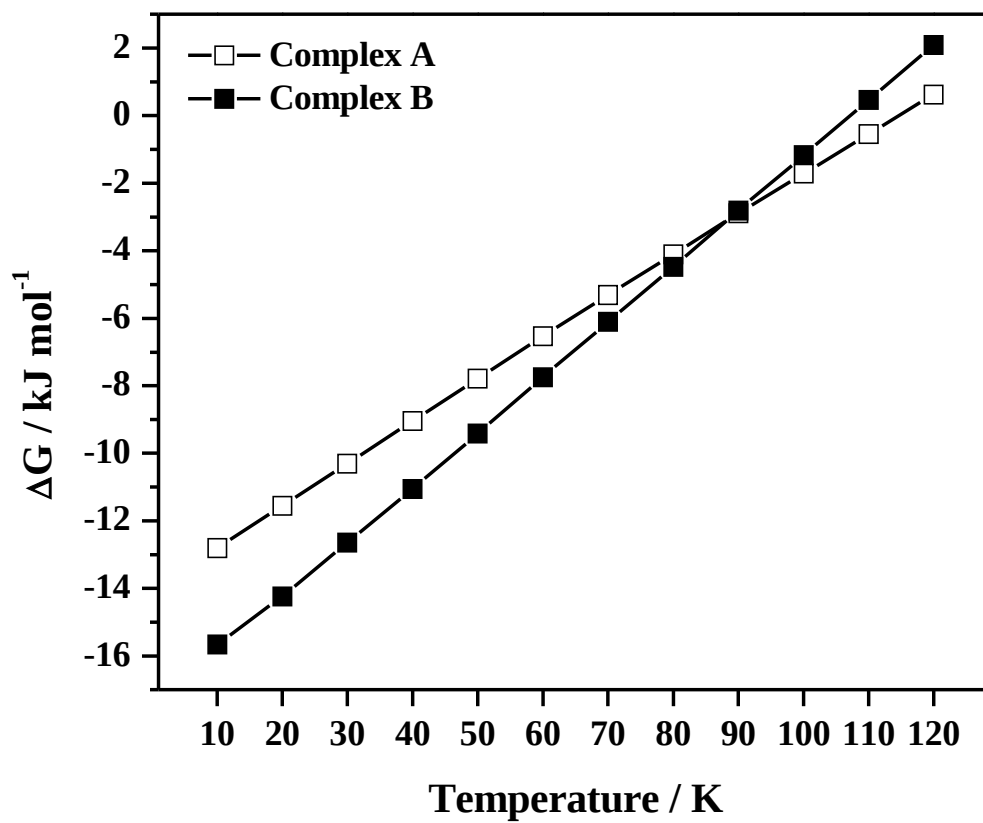


Figure 4. Plot of variation of ΔG vs. T for the formation of the two PHA-BTMA complexes (see text for details).

TABLE 1: Unscaled Vibrational Frequencies (cm⁻¹) of PHA and PHA-BTMA Complexes Calculated at MP2/aug-cc-pVDZ Level of Theory.^a

	$\nu_{\text{C-H}}$	$\nu_{\text{C=C}}$	$\beta_{\text{C-H}}$	$\gamma_{\text{C-H}}$
PHA	3481	2105	606	551
PHA-BTMA (A)	3431	2095	662	592
PHA-BTMA (B)	3476	2101	613	566

^a $\beta_{\text{C-H}}$ = In-plane C–H bend; $\gamma_{\text{C-H}}$ = Out-of-plane C–H bend

TABLE 2: ZPE and BSSE Corrected Stabilization Energies (kJ mol⁻¹) for the PHA-BTMA Complexes Calculated at Various Levels Theory.

	MP2/ aug-cc-pVDZ	CCSD(T)/ aug-cc-pVDZ	DFT-SAPT/ aug-cc-pVDZ	CCSD(T)/ CBS
PHA-BTMA (A)	-12.4	-11.1	-11.4	-16.6
PHA-BTMA (B)	-16.4	-10.9	-11.6	-18.7

TABLE 3: DFT–SAPT Interaction Energy Decomposition (kJ mol⁻¹) for the PHA-BTMA Complexes Calculated using aug-cc-pVDZ Basis Set.

	E_{elec}	E_{ind}	E_{disp}	E_{exch}	δ_{HF}	E_{int}
PHA-BTMA (A)	-20.8	-2.6	-16.4	28.5	-2.7	-14.0
PHA-BTMA (B)	-21.4	-2.5	-34.3	47.3	-3.7	-14.6